applied optics

Low radiation dose calibration and theoretical model of an optical fiber dosimeter for the International Space Station

Diego Di Francesca,[1,2,*] Nicolas Balcon,[3] Pierrick Cheiney,[4] Enrico Chesta,[1] Florence Clement,[3] Sylvain Girard,[2] Julien Mekki,[3] Gilles Melin,[5] Adriana Morana,[2] Martin Roche,[2,3,4] and Daniel Ricci[1]

[1]European Organization for Nuclear Research, CERN, 1211 Geneva 23, Switzerland
[2]Université Jean Monnet, Laboratoire Hubert Curien, 18 rue Pr. Lauras, Saint-Étienne 42000, France
[3]Centre national d'études spatiales, CNES, 18 avenue Edouard Belin, 31401 Toulouse Cedex 9, France
[4]iXblue Navigation System Division, 34 rue de la croix de Fer, 78100 Saint-Germain-En-Layes, France
[5]iXblue Photonics, Rue Paul Sabatier, 22300 Lannion, France
*diego.di.francesca@cern.ch

Received 19 December 2022; revised 21 February 2023; accepted 21 February 2023; posted 24 February 2023; published 23 March 2023

The optical-fiber-based dosimeter of the LUMINA project was deployed in August 2021 in the International Space Station in the framework of the Alpha mission. The sensing elements of the dosimeter are P-doped optical fibers, which were proven to be excellent candidates for dosimetry applications. The twofold objective of this paper is to provide a theoretical model for the radiation response of the dosimeter and to report on the experimental work carried out at CERN for the qualification and calibration of the engineering model of the LUMINA dosimeter. Combining the theoretical response and experimental data, the calibration curve of the flight model is obtained. Finally, this study broadens the investigation of the room temperature radiation response of P-doped optical fibers in a range of dose rates 10^4 times lower than previously reported, from 21 $\mu Gy(SiO_2)/h$ to 145 $mGy(SiO_2)/h$.

https://doi.org/10.1364/AO.483560

1. INTRODUCTION

It is well known that the radiation response of silica-based optical fibers (OFs) is extremely diverse and that some OF types are remarkably sensitive to ionizing radiation [1,2]. One of the most important macroscopic effects observed in OFs is radiation induced attenuation (RIA). This is the darkening effect of the OF, which causes the transmitted light intensity to decrease [2–7]. It is mostly due to the generation of radiation induced point defects, also called color centers, and the appearance of the associated absorption bands in the transmitted spectrum.

The feasibility of an OF dosimeter based on RIA was reported by Evans and Sigel in 1974 [3]. It utilizes the intuitive idea that a very long OF spool would provide correspondingly high radiation sensitivity, a concept that was shortly after used by the same authors to perform the first radiation dose measurements in space with a RIA-based OF sensor.

The OF dosimeter installed on the Navigational Technology Satellite 2 (NTS-2), launched in 1977, is the first application of a RIA-based OF dosimeter in space and one of the earliest applications of OF sensors in space [8]. This dosimeter employed some spools of different lengths of radiation sensitive OF, while a real-time intensity normalization method was applied by means of the usual double-beam reference channel. The radiation resistant channel was used to correct any drift of the injected light power. In their pioneering application, they used an OF with a very complex glass composition, which showed some fading effect of the RIA, a characteristic that can be quite detrimental to the accuracy of the dose measurement.

In the last decades, the study of radiation effects in OFs has been vastly extended, and P-doped OFs emerged as natural candidates for dosimetry applications, as suggested by several authors [5,9–13]. In Ref. [4], Griscom *et al.* provided extensive analysis of P-related radiation induced point defects. By combining optical attenuation (OA) and electron paramagnetic resonance (EPR) measurements, they were able to assign atomic models of such defects and make some hypothesis on the associated generation mechanisms under irradiation. It was shown that a thermally stable absorption band is induced in the near-infrared domain (NIR) at about 1570 nm. Using annealing studies, they demonstrated the correlation of this absorption band with the EPR signature of the P1 defect, an unpaired electron localized on a threefold coordinated P atom. The NIR absorption band was then attributed to the P1 defect. Several years later, dose effect studies at room temperature

provided an independent EPR-OA correlation [14], confirming the original assignment. Similarly, in the visible domain (VIS), the RIA is dominated by the absorption bands associated with the phosphorus oxygen hole center (POHC), which comes in two varieties, metastable POHC and stable POHC, depending on the localization of an unpaired electron on a single nonbridging oxygen (metastable) or on two nonbridging oxygen atoms (stable). It is important to note that in P-doped OFs, the RIA levels in the VIS are usually two orders of magnitudes higher than in the NIR at room temperature, which makes this region very interesting for low dose sensing.

The thermal stability of the P1 defect at room temperature, the monotone response with the dose, the non-dependence on the dose rate, and the ideal spectral localization at telecom wavelengths of the associated band make single mode (SM) P-doped OFs almost ideal for dosimetry [12]. In recent years, their properties have been thoroughly investigated to be employed as distributed radiation in the mixed field environment of high energy particle accelerators [12,13,15]. Although P-doped OF are much more sensitive in the UV-VIS domain than in the NIR, the suitability of such a spectral range for dosimetry application has not received the same amount of validation as applications in the NIR.

The LUMINA project [16], led by the French Space Agency CNES and with the collaboration of iXBlue, the University Jean Monnet, and CERN, aimed at deploying a first demonstrator of a RIA-based OF dosimeter inside the Columbus module of the International Space Station (ISS) [16,17] (shown in Fig. 1). The dosimeter employs P-doped SM OFs produced by iXblue. The low initial OA enables making very long fiber spools, which increase the overall sensitivity and allow the detection of very low radiation doses. The lowest dose rate tested in the present study is 21 μGy(SiO_2)/h, almost 10^4 times lower than the lowest dose rate previously reported in Ref. [12].

Due to the LUMINA project, in the future, the early and reliable detection of rising radiation levels in space satellites will be useful to further reduce the exposure of astronauts to radiation and to mitigate effects on sensitive equipment.

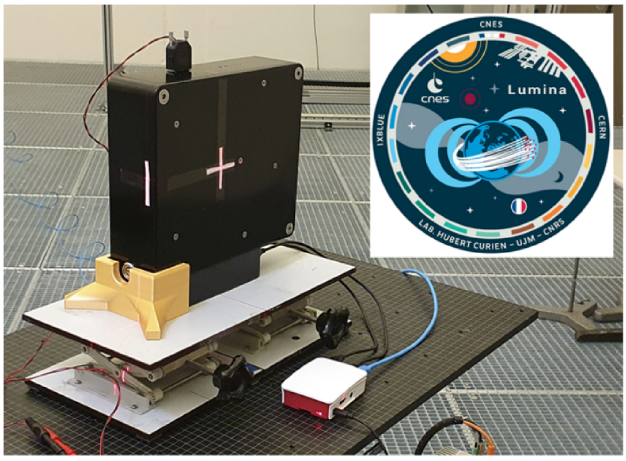

Fig. 1. LUMINA dosimeter in the ^{60}Co irradiation facility at CERN. In the inset, the LUMINA patch.

2. EXPERIMENTAL DETAILS

The experimental activity reported in this contribution was carried out on a dedicated engineering model (EM) of the LUMINA dosimeter demonstrator. The calibration of the flight model (FM), at present collecting data on the ISS, was calculated based on the theoretical model and the experimental results on the EM reported below.

A. Schematic Description of the Sensor

The OF dosimeter is manufactured by iXblue [18]. Its functioning relies on RIA, and it is composed of two independent channels, one operating in the VIS and the second one in the NIR. Some details of the sensor architecture have been reported in Ref. [16] and will be detailed in a future publication.

The optical architecture of the VIS part of the LUMINA dosimeter is analogous to the one reported by Evans *et al*. in Ref [8]. It is constituted by a sensitive channel and a reference channel for the correction of any drift of injected light power (double-beam technique). One of the main differences from Ref. [5] is in the OF sensor itself, which in the case of the present investigation is constituted by a 2 km long P-doped OF, interrogated at 638 nm and is SM at this particular wavelength. The VIS source is a DFB laser with a linewidth of 1 MHz injecting 0.25 mW of optical power. This setup allows performing a direct RIA measurement, i.e., the measurement of the decrease of transmitted light power associated with the radiation dose.

Unlike the VIS part of the LUMINA dosimeter, the NIR part introduces two novelties with respect to Ref. [5]. The sensing element is a 7 km long SM P-doped OF (its composition is very close to that of the fiber in Ref. [12]), and the actual light intensity measurement is carried out in backreflection, as shown in Fig. 1. A continuous beam of infrared light at 1535 nm is injected at one end of the OF. The NIR source is an erbium-based amplified spontaneous emission source with a 20 nm linewidth injecting 0.6 mW of optical power. The injected light is reflected by a mirror at the other end of the OF, and travels backwards for an additional 7 km. The mirror is composed of a silver-coated fiber-end with a flat 98% reflectivity at 1535 nm. Finally, all backscattered light is routed to the photodetector, which measures the output intensity. The relative change of output intensity is related to the RIA, which in turn is supposed to depend linearly on the deposited radiation dose [12]. The injected power is monitored in real time to correct for possible drift or fluctuations. The corresponding reference channel is not shown in Fig. 2.

To further increase the precision of the measurements in both the VIS and NIR, the temperature of each photodetector is monitored by means of thermocouples and used to apply further corrections to the measured intensity.

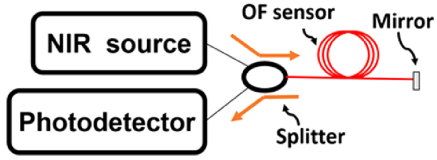

Fig. 2. Schematic representation of the OF dosimeter. For simplicity, the reference channel has been omitted.

Table 1. Irradiation Conditions[a]

	1st Irrad.	2nd Irrad.	3rd Irrad.	4th Irrad.
Dose rate	21 μGy/h	66.6 μGy/h	209 μGy/h	145 mGy/h
Uncertainty (2σ)	1%	1%	1%	4%
Homogeneity	99%	99%	99%	99%
Irrad. time (h)	91.16	64.26	44.39	6.90
Recovery time (h)	122	107	268	181

[a]All doses are in a$-SiO_2$.

B. Calibration Facilities and Irradiation Conditions

The experimental activity to qualify and calibrate the OF dosimeter was carried out in May/June 2021 at the irradiation facilities of CERN. The facilities are equipped with several ^{60}Co sources and all necessary instrumentation to ensure extremely well-controlled irradiation conditions down to average dose rates comparable to the ones in the ISS, ∼200 μGy/day [19].

The irradiation testing consisted of a single data acquisition over the course of 39.4 days. During this period, the acquisition was stopped four times for technical reasons, never for more than 20 min and never during the irradiation phase nor immediately after. During each stop, the EM was relocated inside the facility but always kept powered. T variations during these operations were lower than 3 K.

All irradiations were performed under ^{60}Co γ rays and at temperatures between 295 and 301 K. These temperature irradiation conditions are comparable to the ones of the ISS. Four different dose rates were used, and each irradiation run was followed by a few days of monitoring to detect possible recovery of the RIA. The precise dose rates reported in Table 1 were determined during a thorough calibration of the radiation field carried out the day before the start of the irradiation. The time sequence of the irradiation is plotted in Fig. 3.

The dose rate was progressively increased while decreasing the duration of the irradiation. The last irradiation allowed to reach a total dose of 1 Gy(SiO_2), which is roughly 2.5 times more than the total dose expected for a 5 year long mission on the ISS.

3. THEORETICAL MODEL OF THE DOSIMETER

The VIS part of the LUMINA dosimeter is designed to perform a direct RIA measurement, for which the usual RIA formula is used and that is a straightforward application of the Lambert–Beer law:

$$\mathrm{RIA}(t) = -\frac{10}{L}\log_{10}\left(\frac{I(t)}{I(0)}\right). \tag{1}$$

$I(t)$ is the light intensity transmitted at any time after the start of irradiation, and $I(0)$ is the light intensity before the start of irradiation. For simplicity, the corrections related to the subtraction of noise level and fluctuations of the injected light power are not explicitly reported in Eq. (1). During the calibration procedure, the relation between the irradiation time and the dose is well known, and it is possible to establish a biunivocal relation between the RIA and dose if the fiber sensor behaves as a radiation dose integrator [12].

The NIR part of the LUMINA dosimeter is also based on the RIA effect, but the specific optical architecture is such that the radiation response of the dosimeter is not as direct as the VIS counterpart. The modeling of the sensor response can be done in two steps. The first step is a generic derivation that makes no assumption about the OA of the sensing element or its dependence on the radiation environment. In the second step, we assume that the properties that were demonstrated for this type of P-doped fiber in Ref. [12] also hold at much lower doses and dose rates. The exactitude of this hypothesis can be verified *a posteriori* by comparing the predicted response with the experimentally measured one.

To calculate the radiation response of the dosimeter, it is necessary to evaluate the amount of light that reaches the photodetector for an arbitrary value of OA in the sensing OF. Two main contributions need to be considered.

- First is the light that travels through the OF twice, making a round trip of 14 km. This contribution is attenuated according to the Lambert–Beer law and can be equivalently calculated as the transmitted light over a 14 km long lossy optical link. We will refer to this as *mirror contribution*.
- Second is the light backreflected because of the Rayleigh scattering inside the OF. A certain percentage of light is Rayleigh scattered per unit of traveled length in the OF. A small fraction of it is scattered backwards, re-captured by the OF, and guided to the photodetector. In its journey towards the photodetector, it is attenuated according to Lambert–Beer law, but in this case, the traveled distance varies continuously from 0 to 14 km depending on the scattering position. We will refer to this as *Rayleigh contribution*.

At first glance, the Rayleigh contribution might look negligeable due to the weakness of the scattering process compared to the *mirror reflection*. However, over a long and lossy link, the Rayleigh contribution must become dominant simply because the mirror contribution goes to zero exponentially [20]. The following equation represents the total amount of light that reaches the photodetector:

$$I = I_0\left(e^{-2\int_0^L \alpha \mathrm{d}x} + \int_0^{2L} \alpha_R \beta\, e^{-2\int_0^l \alpha \mathrm{d}x}\mathrm{d}l + \text{negligeable terms}\right). \tag{2}$$

In Eq. (2), I is the output intensity, I_0 is the injected intensity, α is the OA of the OF sensor, L is fiber length (single path), α_R is the loss coefficient due to the Rayleigh scattering, and β

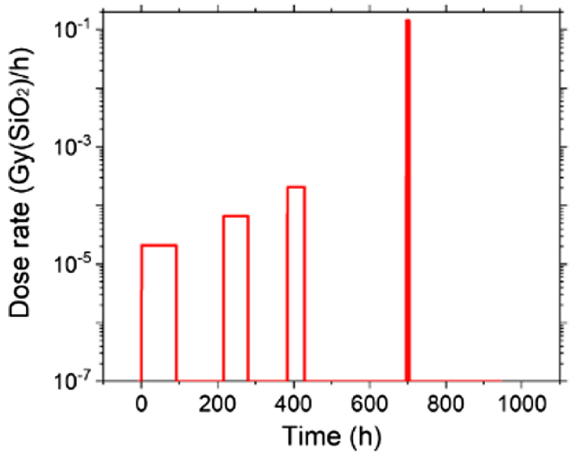

Fig. 3. Irradiation test sequence.

is the fraction of Rayleigh scattered light at position l that is re-captured in the backpropagating direction. The first term in Eq. (2) corresponds to the mirror contribution, i.e., the light traveling 14 km in the OF. The second term in Eq. (2) corresponds to the Rayleigh contribution. Negligeable terms arise from multiple scattering/reflection processes. Assuming that the OA is constant along the OF, it is possible to demonstrate that

$$\frac{I}{I_0} = e^{-2\alpha L} + \frac{\alpha_R \beta}{2\alpha} + \text{negligeable terms.} \quad \textbf{(3)}$$

Equation (3) is derived under the approximation $4\alpha L \gg 1$, which is valid for the system under study, and α constant along the OF. If one of these conditions is not satisfied, a more general version of Eq. (3) can be easily derived from Eq. (2). It is important to note that the second term in Eq. (3) does not depend on the length L of the optical link, and it is inversely proportional to the OA, whereas the first term depends exponentially on the product of L and α. Consequently, the second term becomes dominant for sufficiently high values of the product $2\alpha L$. In the specific case we are studying, the Rayleigh contribution term is about 1.0% of the mirror contribution before the start of irradiation. This was determined experimentally by comparing the measured light power with and without the mirror (α_R and β do not need to be determined separately).

It is now possible to couple Eq. (3) with the RIA response reported in Ref. [12] to address the case of the fiber evenly exposed to radiation. Under the assumptions that (i) the RIA increases linearly with total radiation dose at low doses, (ii) there is no recovery effect, and (iii) RIA is independent from the dose rate, we can re-write Eq. (1) as

$$\frac{I}{I_0} = e^{-2(\alpha_0 + \eta D)L} + \frac{\alpha_R \beta}{2\,(\alpha_0 + \eta D)}. \quad \textbf{(4)}$$

In Eq. (4), α_0 is the OA before the start of irradiation, η is the radiation sensitivity, and D is the total radiation dose. The negligeable terms have been omitted. This equation cannot be solved analytically for D. However, it is invertible and can be used to obtain D via numerical methods. It is important to mention that EM and FM have slightly different initial OAs: for the EM, the initial OA is 1.5 dB/km, whereas for the FM, it is 1.2 dB/km. Consequently, the I/I_0 versus dose curve obtained experimentally for the EM cannot be used directly for the FM. Instead, the calibration curve for the FM must be obtained using Eq. (4) and the appropriate value of α_0, assuming that the radiation sensitivities η of EM and FM are the same.

It should be highlighted that it is not necessary to know all the quantities in Eq. (4) to use it. The information of the RIA is encoded in the relative time change of the output light power, according to the model in Eq. (4), which can be measured experimentally.

As the Rayleigh contribution is about 1% of the mirror contribution before the start of irradiation, it is possible to ignore it for extremely low values (e.g., lower than 50 mGy) of the dose and invert the formula to obtain ηD.

4. EXPERIMENTAL RESULTS

Figure 4(a) shows the RIA measured in the VIS part of the dosimeter as a function of time, whereas Fig. 4(b) shows the same data as a function of dose. The transmitted light quickly reached the noise level during the last irradiation because of the high sensitivity of the OF and limited dynamic range of the detection system. Consequently, the trace in Fig. 4(a) becomes very noisy at high RIA levels. In Fig. 4(b), the x axis has been limited to the first 0.05 Gy to better display the relevant part of the collected data. After the first three irradiations, a noticeable recovery effect takes place. However, it should be noted that around times 107 h, 302 h, and 441 h, the trace in Fig. 4(a) seems to have a brief rapid evolution. These are instrumental artifacts attributed to the operation of momentarily switching off the acquisition during which the compensation of the temperature fluctuations was not perfect.

Figure 5(a) shows the normalized ratio I/I_0 measured in the NIR part of the dosimeter during the four irradiations as a function of time, whereas Fig. 5(b) shows the same data as function of the dose. The inset of Fig. 5(b) highlights the beginning of the curve to better show the data concerning the first three irradiations. A very modest recovery of the transmission was observed following the conclusion of the first three irradiations. This phenomenon was not observed in past studies such as the one reported in Ref. [12], and it was not observed

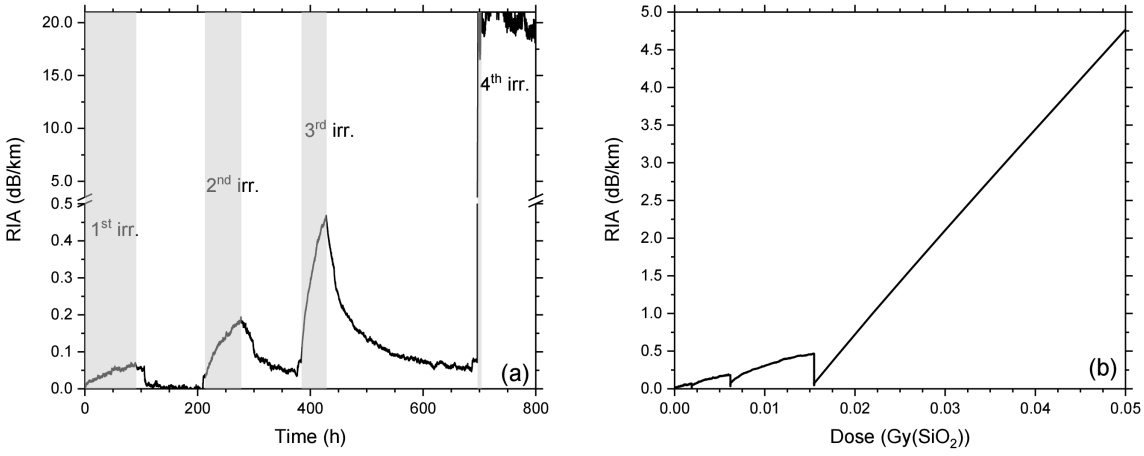

Fig. 4. RIA of the VIS dosimeter as a function of time. (a) First three irradiations. (b) The same curve continues for the fourth irradiation, and the noise level is quickly reached.

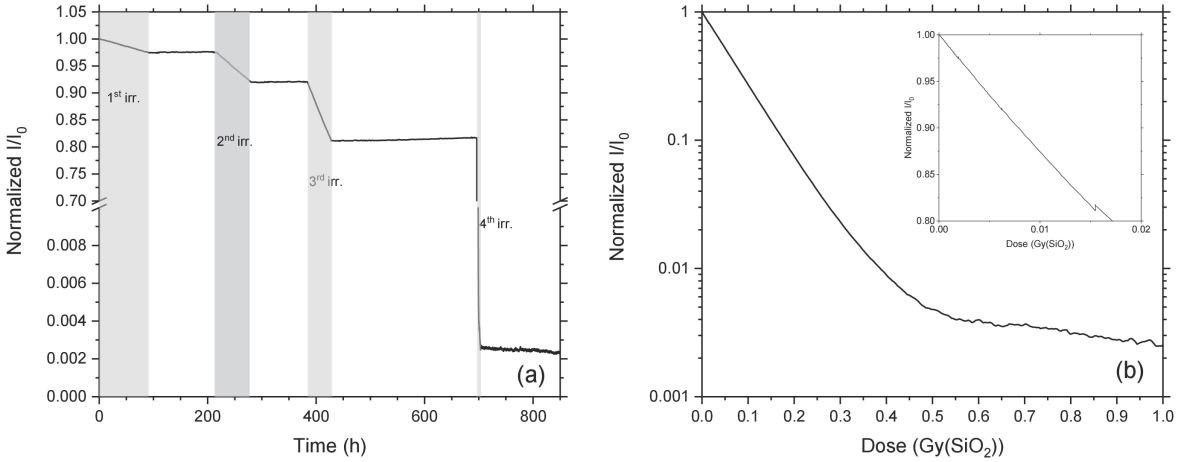

Fig. 5. Radiation response of the NIR OF dosimeter (a) as a function of time and (b) as a function of the dose. The inset in (b) highlights the beginning of the curve in (b).

after the fourth irradiation at total dose of 1 Gy (coherent with the previous investigation in the past). Only the presence of the third recovery is barely visible in the inset of Fig. 5(b) at about 0.15 Gy.

The last technical observation to be reported is that during CERN experimental tests, the full LUMINA dosimeter was exposed to the ^{60}Co irradiation. No system failures were recorded up to the total dose of 1 Gy(SiO_2) in the reported experimental conditions, nor degradation of the performance of any of the dosimeter parts.

5. DISCUSSION

To qualify and calibrate the radiation response of the LUMINA dosimeter, it was decided to perform some irradiations under ^{60}Co γ rays down to dose rates comparable to ISS conditions [19]. To the best of the authors' knowledge, this work sheds light for the first time on the RIA behavior of P-doped OFs at doses and dose rates as low as the ones investigated here. Moreover, this study lays the groundwork to better understand the suitability of γ rays in predicting RIA in ISS-like environments for any OF type. Although it will not be possible to extrapolate the results of this work to all OF types, the fact that P-doped OFs can be calibrated is very advantageous when understanding the environment variables compared to other OF types for which the radiation response is hardly predictable already in better-controlled conditions.

The VIS part of the LUMINA dosimeter has shown an important recovery effect after the end of the first three irradiations. The authors' current hypothesis is that the recovery is largely due to a photobleaching effect, which is going to be considered in the actual operation of the FM of the dosimeter. The origin of this recovery has not been deeply investigated at this time and will be studied further in the future. It should also be noted that the first three irradiations reported in Fig. 4 show a complex dependence on the dose and dose rate. This is not strange if we consider the competition between the defect generation processes and the evidenced recovery mechanisms. During the fourth irradiation, the response of the VIS dosimeter appears much more linear with the dose because the much higher dose rate dominates the radiation response of the sensor. In this case, it is possible to perform a linear fit in the dose range between 0.02 and 0.04 Gy to obtain a reference value of the radiation sensitivity in these specific irradiation conditions. The radiation sensitivity obtained is then $137 \pm 6\,\mathrm{dB \cdot km^{-1} \cdot Gy^{-1}}$. The error bar considers the 4% uncertainty deriving from the irradiation conditions (see Table 1), which weighs much more than the error due to the linear regression procedure.

It is evident that the RIA response of the VIS dosimeter recorded during the tests deviates from the ideal behavior outlined in Ref. [12]. Apart from the possible corrective measures that can be implemented to improve the behavior of the sensor, it should be noted that this OF remains a very valuable radiation sensor and that it provides useful information on the dose. This is especially true if the recorded data can be complemented with those from other nearby sensors and, specifically, in the case where a rapid increase of the dose rate needs to be detected. For example, on ISS, a significant increase of the dose rate is caused by the recurrent passage through the South Atlantic Anomaly (SAA), as well as a sudden increase of solar activity. In applications other than ISS, short-term stability can also be sufficient to retrieve the needed dose information. For example, in Ref. [21], Paillet *et al*. have reported a rather stable RIA at 620 nm after 14 MeV neutron irradiation pulses in multimode P-doped OFs.

In Table 2, we report the measured value of the RIA for each of the different irradiations of the NIR dosimeter. The obtained values are compatible with each other and with the previously reported results in Ref. [12] for a SM OF of comparable composition. Table 2 also contains the measured recovery values after the stop of each irradiation over a few days. For the first three irradiations, the recovery is positive, meaning the RIA did slightly decrease, whereas in the fourth irradiation, up to 1 Gy, the recovery is negative, meaning that the attenuation keeps increasing after irradiation stops. Such a phenomenon of consolidation of the RIA, limited to a very few percentage points, was also observed in the past [6,12]. This is attributed to the conversion mechanism of POHC defects to the more stable P1 defects, which are also hole centers.

In Fig. 6, the analysis of the NIR dosimeter data is reported. In Fig. 6(a), the experimental calibration of normalized ratio

Table 2. RIA and Recovery of the NIR Dosimeter for Each Irradiation

Dose Rate (mGy(SiO2))	Sensitivity ($dB \cdot km^{-1} \cdot Gy^{-1}$)	Error (2σ)	Total Cumulated Dose	Recovery Time (h)	Measured Recovery (%)
21 µGy/h	4.24	1%	1.914	122	0.15
66 µGy/h	4.24	1%	6.194	107	0.10
209 µGy/h	4.22	1%	15.5	268	0.7
145 mGy/h	3.96	4%	1015.5	181	−9.5

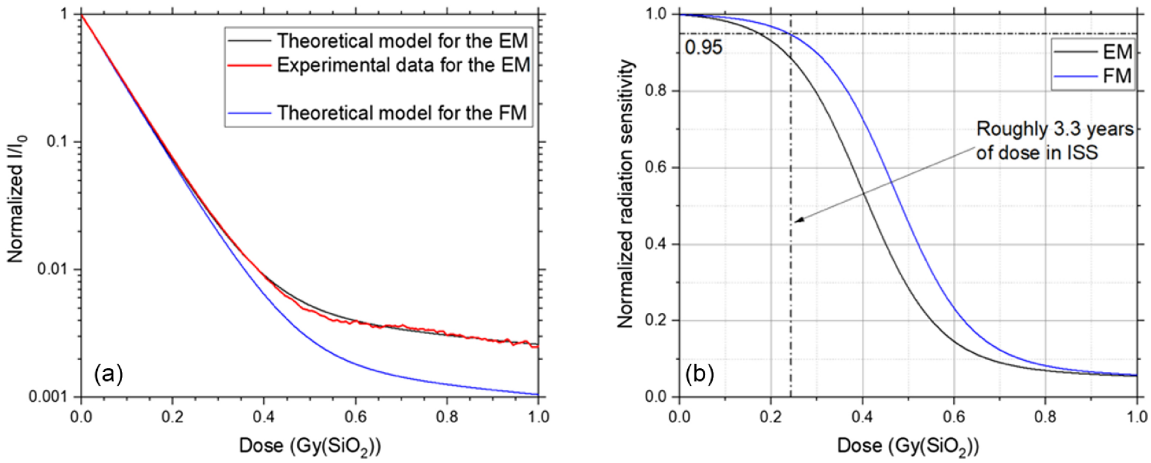

Fig. 6. (a) Theoretical model and calibration data of the NIR part of the EM, as well as the calculated calibration curve for the FM. (b) Respective sensitivities of EM and FM.

I/I_0 is shown as a function of the dose together with the corresponding predicted response obtained from the theoretical model [Eq. (4)]. In the same figure, the expected calibration curve of the FM is also shown. In these calculations, the value of the radiation sensitivity η was set equal to 4.2 $dB \cdot km^{-1} \cdot Gy^{-1}$. The match between experimental data and predicted model is excellent, and it proves that the assumption of constant radiation sensitivity from 0 to 1 Gy and dose rate independence is substantially correct.

In Fig. 6(b), the respective normalized sensitivities of the NIR dosimeter have been calculated for both EM and FM. Because of the interplay between the mirror contribution and Rayleigh contribution, the sensitivity is sigmoidal shaped and drops considerably for doses higher than 0.2 or 0.3 Gy. In the case of the FM, it has been calculated that a 5% loss in sensitivity will happen after about 3.3 years of operation on the ISS under average irradiation conditions. The difference between the EM and FM calibration curves in Fig. 6 is due entirely to the different initial OA of the fiber sensors, which are 1.5 and 1.2 $dB \cdot km^{-1}$, respectively. The choice of using the OF sensor with lower initial OA for the actual ALPHA mission extends significantly the high-sensitivity region of the sensor. After a total dose of only 0.9 Gy, both EM and FM dosimeters become much less sensitive to additional radiation doses. This is due to the Rayleigh contribution in Eq. (4), becoming the dominant contribution to the I/I_0 with respect to the exponentially decreasing mirror contribution.

As briefly mentioned above, the calibration carried out under ^{60}Co γ rays on the EM is used to derive the best calibration curve of the FM. A key hypothesis is that the fiber sensors in the EM and FM are identical (except for the value of the initial OA) and respond identically to the same radiation field. Although the latter hypothesis was not verified at the lowest dose levels investigated here, it has been proven to be correct down to 4 mGy/h under γ rays on shorter lengths (200 m) of the OF [22]. Although the radiation sensitivity reported by the authors in Ref. [22] are slightly larger, they were satisfied with the agreement they obtained with Ref. [12], which is substantially coherent with this work.

The overall performance of the NIR part of the dosimeter provided very promising results. P-doped OFs preserve excellent RIA-based dosimetry properties down to dose rates 10^4 lower than those investigated before. This result alone paves the way for the further development and application of P-doped OFs as dosimeters in new environments, such as space. The predictable RIA behavior also allows to design and properly size the optical architecture of a sensor as the one in Fig. 2. The backreflection interrogation scheme of the LUMINA dosimeter allowed to almost double the sensitivity of a given fiber length at least for the first 3.3 years of operation on ISS. After this initial period, the sensitivity decreases in a controlled and predictable way, reaching a sensitivity at 0.4 Gy (comparable to 5 years of operation on ISS) that is still 1.5 times higher than the one of a dosimeter employing a 7 km long fiber in transmission.

It is very relevant to notice how the overall performance of the dosimeter depends non-trivially on the actual optical architecture. For example, using a significantly longer fiber would cause a degradation of the sensitivity instead of an improvement. This is because the Rayleigh contribution in Eq. (4) would weight more with respect to the mirror contribution already in the initial phases of irradiation. The transition from high sensitivity to low sensitivity would occur at lower doses too. The initial

OA also plays a primary role similar to the fiber length. A small initial difference in this manufacturing parameter can drastically impact the performance. To understand it, it is sufficient to notice that an initial OA of 2 $dB \cdot km^{-1}$, instead of 1.5 or 1.2, would be equivalent to performing pre-irradiation to a dose of 0.2 Gy. In Fig. 6(b), such a dose already corresponds to the start of the transition to lower sensitivity.

Finally, based on the results of this work, it is intriguing to speculate on the performance of a dosimeter with the same architecture as in Fig. 2, but without the mirror at the end of the long OF sensor. Of course, the *mirror term* would disappear from all equations reported above, and the performance would rely entirely on the Rayleigh term:

$$\frac{I}{I_0} = \frac{\alpha_R \beta}{2\,(\alpha_0 + \mathrm{RIA})}, \tag{5}$$

$$\mathrm{RIA} = \frac{\alpha_R \beta}{2\frac{I}{I_0}} - \alpha_0. \tag{6}$$

The usual logarithmic dependence of the RIA from the ratio I/I_0 [as in Eq. (1)] that derives directly from the Lambert–Beer law disappears, and it is replaced by a hyperbolic dependence. Such a radiation response might not be ideal to monitor environments such as the ISS but would be interesting for others. More generally, this is a clear example of how to drastically, and possibly dynamically, change the performance of an OF-based dosimeter by changing its optical architecture and not the OF sensor itself. This concept could be exploited to further develop and tailor OF-based dosimeters in the future.

6. CONCLUSIONS

We report on the calibration of an OF sensor for radiation dosimetry deployed on the ISS in 2021. The significance of this work is threefold. From a physical standpoint, we extend the study of radiation effects in P-doped silica-based SM OFs in a range of doses and dose rates never investigated before. We showed that P-doped OFs preserve excellent dosimetry properties if interrogated in the NIR, at least for systems operating at room temperature. We derived a theoretical model of the mirror-assisted sensor performance. From an experimental standpoint, we reported the results of the qualification and calibration work carried out at CERN, which showed an excellent match with the prediction of the theoretical model, and the robustness of the full dosimeter against total ionizing dose effects. Finally, from an engineering standpoint, we have highlighted how the optical architecture of the dosimeter has a major impact on the actual performance. This concept shall be exploited in the future to build even more sensitive OF-based dosimeters.

Acknowledgment. The authors acknowledge the support of ESA, the R2E project, and the KT and RP groups at CERN.

Disclosures. The authors declare no conflicts of interest.

Data availability. Data underlying the results presented in this paper are not publicly available at this time but may be obtained from the authors upon reasonable request.

REFERENCES

1. E. J. Friebele, M. E. Gingerich, and K. J. Long, "Radiation damage of optical fiber waveguides at long wavelengths," Appl. Opt. **21**, 547–553 (1982).
2. S. Girard, A. Alessi, N. Richard, L. Martin-Samos, V. De Michele, L. Giacomazzi, S. Agnello, D. Di Francesca, A. Morana, B. Winkler, I. Reghioua, P. Paillet, M. Cannas, T. Robin, A. Boukenter, and Y. Ouerdane, "Overview of radiation induced point defects in silica-based optical fibers," Rev. Phys. **4**, 100032 (2019).
3. B. D. Evans and G. H. Sigel, "Permanent and transient radiation induced losses in optical fibers," IEEE Trans. Nucl. Sci. **21**, 113–118 (1974).
4. D. L. Griscom, E. J. Friebele, K. J. Long, and J. W. Fleming, "Fundamental defect centers in glass: Electron spin resonance and optical absorption studies of irradiated phosphorus-doped silica glass and optical fibers," J. Appl. Phys. **54**, 3743–3762 (1983).
5. H. Henschel, O. Köhn, and H. U. Schmidt, "Optical fibres as radiation dosimeters," Nucl. Instrum. Meth. Phys. Res. B **69**, 307–314 (1992).
6. P. Borgermans, B. Brichard, F. Berghmans, F. Vos, and M. Decreton, "On-line gamma dosimetry with phosphorous and germanium co-doped optical fibres," RADECS **99**, 477–482 (1999).
7. T. Wijnands, K. Aikawa, J. Kuhnhenn, D. Ricci, and U. Weinand, "Radiation tolerant optical fibers: from sample testing to large series production," J. Lightwave Technol. **29**, 3393–3400 (2011).
8. B. D. Evans, G. H. Sigel, J. B. Langworthy, and B. J. Faraday, "The fiber optic dosimeter on the navigational technology satellite 2," IEEE Trans. Nucl. Sci. **25**, 1619–1624 (1978).
9. R. H. West, "P-doped optical fibres in dosimetry," SPIE Remote Sens. **4547**, 61–68 (2002).
10. M. C. Paul, D. Bohra, A. Dhar, R. Sen, P. K. Bhatnagar, and K. Dasgupta, "Radiation response behavior of high phosphorous doped step-index multimode optical fibers under low dose gamma irradiation," J. Non-Cryst. Solids **355**, 1496–1507 (2009).
11. S. Girard, Y. Ouerdane, C. Marcandella, A. Boukenter, S. Quenard, and N. Authier, "Feasibility of radiation dosimetry with phosphorus-doped optical fibers in the ultraviolet and visible domain," J. Non-Cryst. Solids **357**, 1871–1874 (2011).
12. D. Di Francesca, G. Li Vecchi, S. Girard, A. Morana, I. Reghioua, A. Alessi, C. Hoehr, T. Robin, Y. Kadi, and M. Brugger, "Qualification and calibration of single-mode phosphosilicate optical fiber for dosimetry at CERN," J. Lightwave Technol. **37**, 4643–4649 (2019).
13. H. Henschel, M. Körfer, J. Kuhnhenn, U. Weinand, and F. Wulf, "Fibre optic radiation sensor systems for particle accelerators," Nucl. Instrum. Methods Phys. Res. A **526**, 537–550 (2004).
14. D. Di Francesca, S. Girard, S. Agnello, A. Alessi, C. Marcandella, P. Paillet, Y. Ouerdane, Y. Kadi, M. Brugger, and A. Boukenter, "Combined temperature radiation effects and influence of drawing conditions on phosphorous-doped optical fibers," Phys. Status Solidi A **216**, 1800553 (2019).
15. D. Di Francesca, A. Infantino, G. Li Vecchi, S. Girard, A. Alessi, Y. Kadi, and M. Brugger, "Dosimetry mapping of mixed-field radiation environment through combined distributed optical fiber sensing and FLUKA simulation," IEEE Trans. Nucl. Sci. **66**, 299–305 (2019).
16. F. Clément, P. Cheiney, S. Girard, D. Di Francesca, N. Balcon, A. Morana, M. Roche, M. Jean-Christophe, L. O. Marot, D. Ricci, J. Mekki, R. Canton, and G. de la Fuente, "Lumina, a fiber optic dosimeter aboard the ISS since alpha mission," in *73rd International Astronautical Congress*, Paris, France, 2022.
17. D. Di Francesca, N. Balcon, P. Cheiney, E. Chesta, F. Clement, S. Girard, J. Mekki, G. Melin, A. Morana, M. Roche, and D. Ricci, "Theoretical model and calibration of an optical fibre dosimeter for the International Space Station," in *27th Optical Fiber Sensors Conference*, Alexandria, Virginia, USA, 2022.
18. https://www.ixblue.com/.
19. T. Berger, B. Przybyla, D. Matthiä, *et al.*, "DOSIS & DOSIS 3D: long-term dose monitoring onboard the Columbus Laboratory of the International Space Station (ISS)," J. Space Weather Space Clim. **6**, A39 (2016).
20. A. H. Hartog, *An Introduction to Distributed Optical Fibre Sensors*, 1st ed. (CRC Press/Taylor and Francis, 2018).

21. P. Paillet, S. Girard, V. Goiffon, O. Duhamel, A. Morana, D. Lambert, V. De Michele, C. Campanella, G. Mélin, T. Robin, J. Vidalot, A. Meyer, A. Boukenter, Y. Ouerdane, E. Marin, V. Y. Glebov, and G. Pien, "Phosphosilicate multimode optical fiber for sensing and diagnostics at inertial confinement fusion facilities," IEEE Sens. J. **22**, 22700–22706 (2022).

22. A. Meyer, A. Morana, L. Weninger, N. Balcon, G. Mélin, J. Mekki, T. Robin, A. Champavère, F. Saigné, J. Boch, T. Maraine, A. Aït-Ali-Saïd, E. Marin, Y. Ouerdane, A. Boukenter, and S. Girard, "Towards an embedded and distributed optical fiber-based dosimeter for space applications," IEEE Trans. Nucl. Sci. (2022).